


Article

Confinement Effects on Chemical Equilibria: Pentacyano(Pyrazine)Ferrate(II) Stability Changes within Nanosized Droplets of Water

Teofilo Borunda ¹, Alexander J. Myers ¹, J. Mary Fisher ², Debbie C. Crans ^{2,*} 
and Michael D. Johnson ^{1,*}

¹ Department of Chemistry & Biochemistry, New Mexico State University, Las Cruces, NM 88003, USA; teo2491.tb@gmail.com (T.B.); amwy6@mail.missouri.edu (A.J.M.)

² Department of Chemistry, Colorado State University, Ft. Collins, CO 80523, USA; maryjfisher@gmail.com

* Correspondence: Debbie.Crans@colostate.edu (D.C.C.); johnson@NMSU.Edu (M.D.J.);
Tel.: +1-970-491-7635 (D.C.C.); +1+575-646-3627 (M.D.J.)

Academic Editors: Pallavincini Piersandro and Giacomo Dacarro

Received: 5 March 2018; Accepted: 4 April 2018; Published: 9 April 2018



Abstract: Nanoscale confinement is known to impact properties of molecules and we observed changes in the reactivity of an iron coordination complex, pentacyano(pyrazine)ferrate(II). The confinement of two coordination complexes in a sodium AOT/isooctane reverse micellar (RM) water droplet was found to dramatically increase the hydrolysis rate of $[\text{Fe}(\text{CN})_5\text{pyz}]^{3-}$ and change the monomer-dimer equilibria between $[\text{Fe}(\text{CN})_5\text{pyz}]^{3-}$ and $[\text{Fe}_2(\text{CN})_{10}\text{pyz}]^{6-}$. Combined UV-Vis and $^1\text{H-NMR}$ spectra of these complexes in RMs were analyzed and the position of the monomer-dimer equilibrium and the relative reaction times were determined at three different RM sizes. The data show that the hydrolysis rates (loss of pyrazine) are dramatically enhanced in RMs over bulk water and increase as the size of the RM decreases. Likewise, the monomer-dimer equilibrium changes to favor the formation of dimer as the RM size decreases. We conclude that the effects of the $[\text{Fe}(\text{CN})_5\text{pyz}]^{3-}$ stability is related to its solvation within the RM.

Keywords: Confinement effects; coordination chemistry at the nanoscale; pentacyano(pyrazine) ferrate(II); $[\text{Fe}(\text{CN})_5\text{pyz}]^{3-}$; hydrolysis rates; monomer-dimer equilibrium; reverse micelles; interface interactions

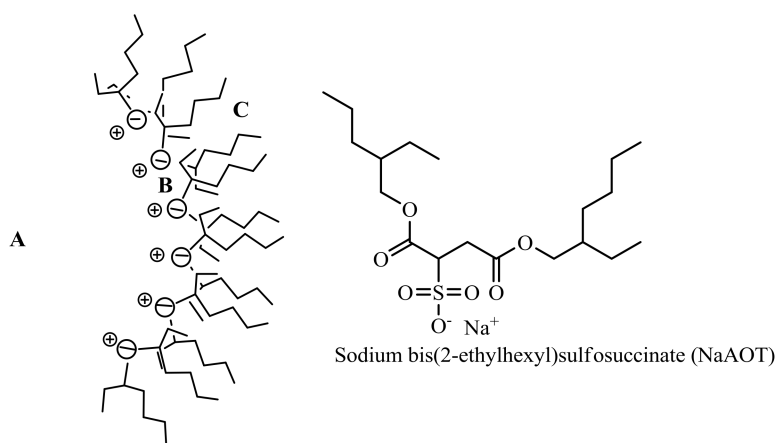
1. Introduction

Coordination complexes undergo ligand exchange reactions that are critical for their chemical reactivity in catalytic processes [1–4]. Mechanistic studies of metal–ligand complexation reactions have been reported for bulk solvent systems, water in particular, and are the basis for our understanding of how metal complexes behave in solution [5–12]. While such studies have provided an understanding of the fundamental ligand exchange reaction mechanisms, and hence metal ion speciation and behavior, they may not capture all the effects present in systems where inhomogeneous bulk solvation of metal ions governs the system properties. This may be particularly true for example at enzyme active sites, and at interfaces where chemical reactivity may be different from that found in bulk solvent media. Conditions where reaction solvation has been altered by “confinement” generally results in changes in chemical reactivity [13–17]. Fendler et al. reported accelerated substitution aquation rates for chromium(III) and cobalt(III) amine complexes in reverse micelles (RM) [18,19]. The increased substitution rates were attributed to association of the coordinated ligand with the surfactant RM interfaces and solvation changes. In other reports, small accelerations in ligand substitution rates at pentacyano(ligand)ferrate(II) centers were reported [20]. The substitution reactions of labile cobalt(II)

complexes were also determined [21,22] and the observed differences in their substitution rates and speciation within RMs were ascribed to the cobalt complex residing at the interface where its solvation is different than in bulk solvents. This may also hold true for the iron pentacyano(ligand)ferrate(II) studies described above. We have previously found that compounds can either be more stable [23,24] or hydrolyze [25] in the vicinity of a reverse micellar interface. It is important to investigate such systems to understand the underlying factors affecting the reactions of complexes in nanoenvironment.

We have initiated a series of studies of how chemical reactivity of transition metal complexes is affected when placed into RMs, where the probe of interest is confined within a nano-sized water pool or near its interface [26–28]. These studies have shown both rate enhancement and diminution, depending on the system under investigation. The rate changes have been ascribed due to differences in the location of the probe molecules (complexes and free ligands) as well as changes in their fundamental physical properties, i.e., pKa values [29] or redox potentials [30]. As a result of these studies, it has become clear that more detailed information on simple substitution reactions at metal centers in coordination complexes is essential to understand the molecular reactivity modifications we have observed.

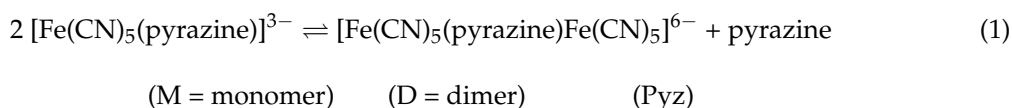
RMs are self-assembled structures formed when small amounts of water are added to a solution of a surfactant in an organic solvent. A large number of such systems can be formed, the most studied and best characterized system consist of sodium bis(ethylhexyl)sulfosuccinate (NaAOT), organic hydrocarbon solvent, and water [31–38]. Combining these three components, the surfactant rapidly self-assembles to surround the water droplets as RMs suspended in the organic solvent. The structure of NaAOT and a representative “slice” of the structure of a NaAOT RM interface is shown in Scheme 1. Although the image represents a seemingly rigid spherical structure, the system is thermodynamically stable but water and potential probes and surfactants are exchanging rapidly between RMs. Importantly, droplet size, and hence water content, is easily changed in a controlled manner. Specifically, the water droplet size is directly proportional to the ratio of water to surfactant ($w_0 = [\text{H}_2\text{O}]/[\text{surfactant}]$) [29,32,39].



Scheme 1. The structures of the reverse micellar interface of a NaAOT reverse micelle (RM) with three different specific locations for additives. Labels A, B, and C shown are in the aqueous core, interfacial region, and hydrophobic part of the nanostructure, respectively. (left) and the structure of NaAOT (right).

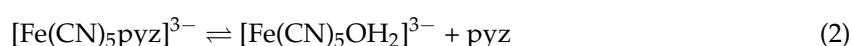
Coordination complexes of transition metal ions can be particularly sensitive to their environment, so their confinement within nanosized water droplet cores of RMs allows a change in speciation [40,41]. Since ligand exchange will be sensitive to environment, confinement could change the complexation equilibria as a result of interaction with the interface, smaller water pool, or both [42]. Characterization of systems that may undergo speciation changes are thus desirable in order to examine if their changes in molecular properties are associated with information on the location of the compounds in these

RM systems. In the following, we report the partial loss of pyrazine and subsequent dimerization of pentacyano(pyrazine)ferrate(II), as shown below in Equation (1), along with the effect of the size of the RM on the position of this equilibrium. These studies are important because they demonstrate how these nanosized nonhomogeneous environments can change the equilibria in coordination complexes important in catalytic reactions.



2. Results and Discussion

Aqueous solutions of sodium pentacyano(pyrazine)ferrate(II) are relatively stable and decompose slowly ($k_d = 4.2 \times 10^{-4} \text{ s}^{-1}$) with the release of pyrazine as shown in Equation (2) [43].



As noted, the products and reactants are in equilibrium with each other ($K_f = 90$) with a reformation rate constant of $k_f = 3.8 \times 10^2 \text{ M}^{-1} \text{ s}^{-1}$ [43]. The well-known aquation rates, coupled with a high molar extinction coefficient of the MLCT band at 458 nm, $3 \times 10^3 \text{ M}^{-1} \text{ cm}^{-1}$ [20], make $[\text{Fe}(\text{CN})_5\text{pyz}]^{3-}$ an excellent system to study the effects of confinement on the stability of coordination complexes. In addition, the pK_a of free pyrazine is 0.6, and the pK_a of complexed pyrazine is even lower, making this equilibrium relatively pH insensitive.

2.1. Kinetic Measurements Using UV-Vis Spectroscopy

When $\text{Na}_3[\text{Fe}(\text{CN})_5\text{pyz}]$ is dissolved in water at $\sim 5 \times 10^{-4} \text{ M}$ concentration, the MLCT peak at 458 nm slowly disappears as the pyrazine is lost from the first coordination sphere, see Figure 1. The extent of hydrolysis of the metal complex in water and upon confinement within a large AOT RM can readily be monitored using UV-Vis in the absence and the in presence of compound. Both sets of spectra were recorded over a 2-h timeframe and shown in Figure 1.

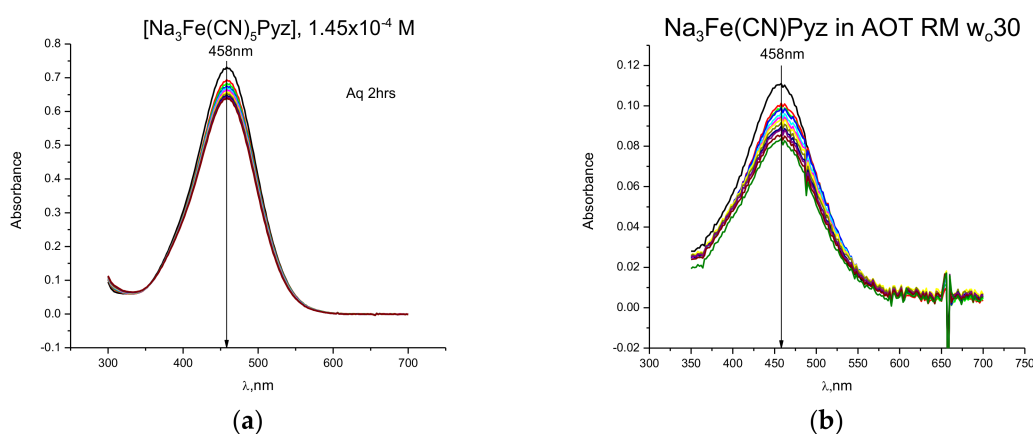


Figure 1. Hydrolysis of aqueous (a) and confined solutions (b) of an iron-pyrazine complex in 200 mM AOT in isoctane. The concentration of $\text{Na}_3[\text{Fe}(\text{CN})_5\text{pyz}]$ is $2.45 \times 10^{-4} \text{ M}$ and approximately m in the AOT/isoctane RM suspension.

In a large RM, w_0 30, the hydrolysis rate is very similar to bulk water, see Figure 1. It is important to note that the position of the peak remains at 458 nm which suggests that the pyrazine portion of the complex has not penetrated the negatively charged interfacial region of the AOT-RM matrix. The extinction coefficients (calculated as probe molarity within the entire sample, not just the RM pool)

in and out of a RM are identical, again supporting the location of the probe within the water pool. It is well known that MLCT complexes such as these are very sensitive to their environment and that penetration/insertion into the interface should result in a change of the MLCT band [11,20]. This is, in fact, what is observed with other MLCT complexes in a range of different RMs [20].

When the probe molecule is confined within a smaller RM, differences are immediately observed. Figure 2 shows the hydrolysis of the iron-pyrazine complex in two smaller AOT RMs with w_0 sizes 20 and 5. At w_0 20, the hydrolysis occurs more extensively than in bulk water, over a two-hour time frame, and with the slight appearance of a red-shifted shoulder. When the size of the RM is small, w_0 5, the hydrolysis is complete within two hours and the shoulder observed at w_0 20 is now resolved into a new peak at 506 nm. The observed peak position corresponds to the literature value for the dimer, $[\text{Fe}_2(\text{CN})_{10}(\text{pyz})]^{6-}$ [44].

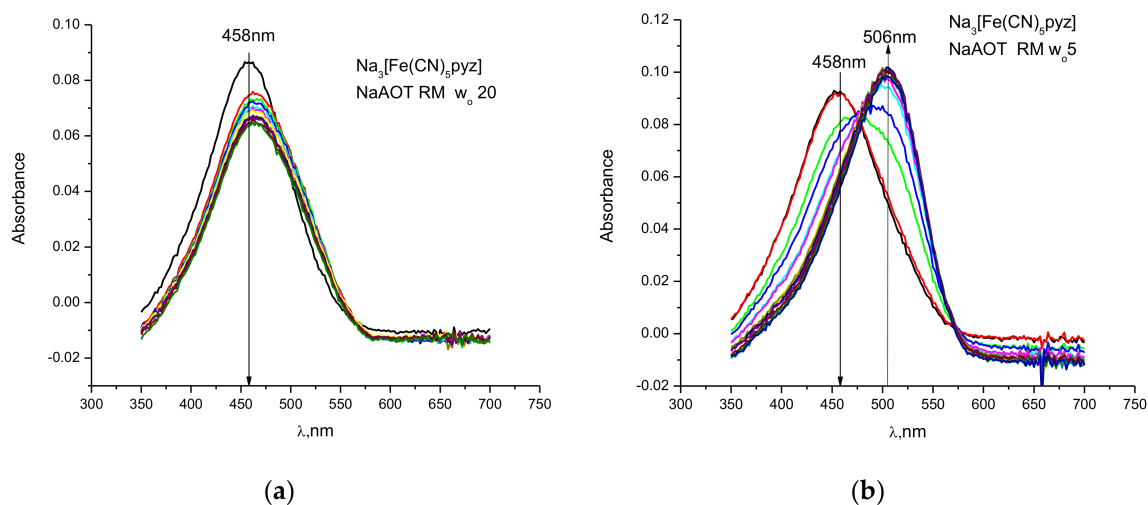


Figure 2. Hydrolysis of $[\text{Fe}(\text{CN})_5\text{pyz}]^{3-}$ in w_0 20 (a) and in w_0 5 (b) AOT/isooctane. The water concentration of $[\text{Fe}(\text{CN})_5\text{pyz}]^{3-}$ is approximately 10^{-4} M.

The observed spectra may be explained by the initial hydrolysis of some of the starting material into pyrazine and the pentacyanoaquaferate(II) complex. This aqua intermediate then rapidly adds to the remaining starting material to form the pyrazine bridged dimer.



The formation of the pyrazine dimer in simple aqueous solutions is readily measured. However, in RMs the conversion is more complex and the kinetic measurements are difficult to make. We suggest the complexities are due to a potential loss of cyanide from the iron center [11] or the formation of the oxo(hydroxo)bridged iron dimer, $[(\text{CN})_5\text{Fe}-\text{O}(\text{H})-\text{Fe}(\text{CN})_5]^{(7-)/8-}$ initially formed from the aqua species [11].

Attempts to suppress the dimerization process were carried out by trapping the aqua intermediate with sodium cyanide, thereby converting it into the substitution inert hexacyanoferrate(II). In aqueous media with 0.050 M cyanide, the simple loss of the peak at 458 nm was observed. Figure 3 shows the same reaction carried out in a w_0 5 RM. Even under these conditions, dimer formation occurs, albeit to a much lesser extent. This observation supports the interpretation that the pyrazine bridged dimer is thermodynamically favored in the small RMs.

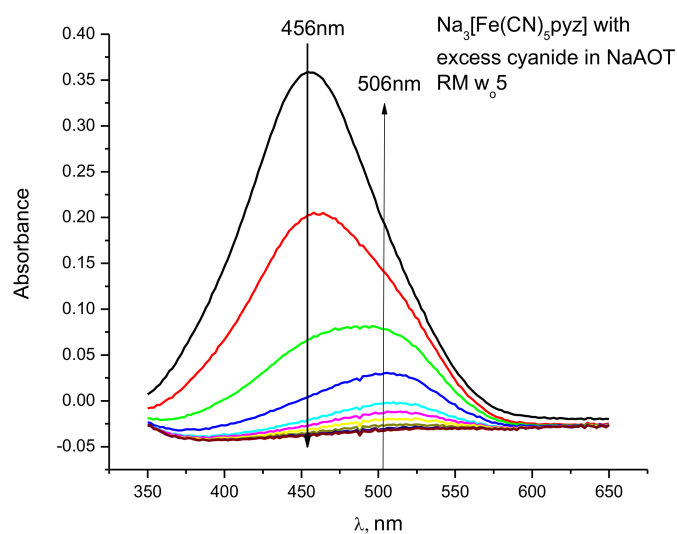


Figure 3. Trapping experiments for $[\text{Fe}(\text{CN})_5\text{OH}_2]^{3-}$ with 0.05M sodium cyanide in the water droplet in a w_0 5 AOT/isooctane RM. The concentration of $[\text{Fe}(\text{CN})_5\text{pyz}]^{3-}$ is approximately 5×10^{-5} M.

Finally, starting with the pyrazine bridged dimer and dissolving it into water, the peak at 506 nm decreased and was replaced by a peak at 458 nm, corresponding to formation of the monomer. This is in stark contrast to observations with the dimer confined within a w_0 20 RM, see Figure 4. During the same time-period while the dimer hydrolyzed in bulk water, the dimer appeared to be more stable with only observation of about ~20% decomposition. These results provide evidence that the dimer's stability is greatly enhanced upon confinement within an AOT RM. Additional information on where the complexes are located is desirable upon placement into the RMs.

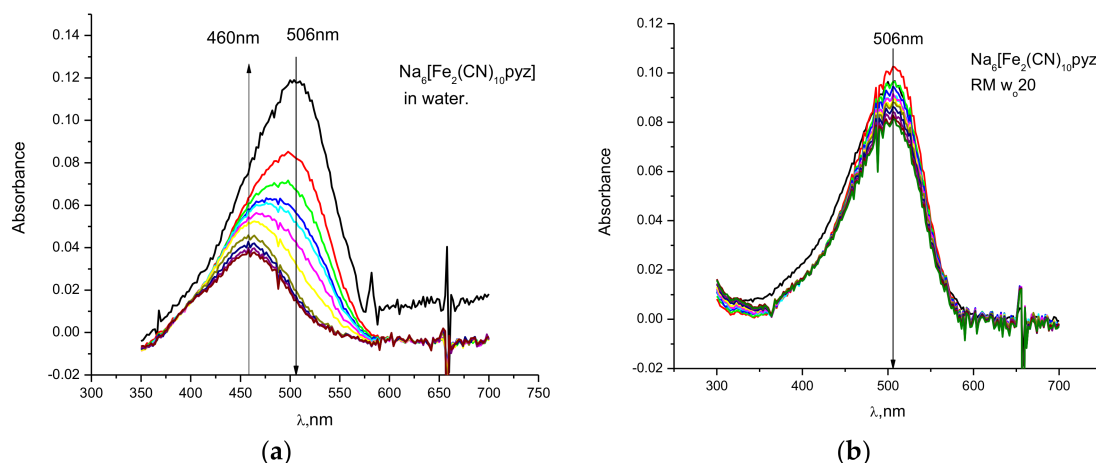


Figure 4. Hydrolysis of the $\sim 5 \times 10^{-5}$ M iron-pyrazine dimer in water (a) and a w_0 20 AOT/isooctane RM (b). The reaction was monitored for about 2 h.

2.2. Thermodynamic Measurements using ^1H -NMR Spectroscopy

To gain further insight into these reactions in nanodroplets, we used ^1H -NMR spectroscopy to determine the location of the components and the equilibrium constants. In Figure 5, the ^1H -NMR spectra are shown for the iron monomer (abbreviated M on the figures), dimer (abbreviated D on the figures), and free pyrazine, (abbreviated Pyz on the figures) in D_2O and a large and small RM, respectively. In Figure 5, the bottom three spectra provide for the assignment of the resonances of each species in D_2O (M, D, and Pyz). The monomer shows the expected doublets at 9.09 and 8.22 ppm from

the coordinated pyrazine, along with two other resonances at 8.65 and 8.63 ppm [45]. The signal at 8.63 ppm is assigned to free pyrazine and the dimer shows a singlet at 8.65 ppm. This assignment is further confirmed from spiking experiments where free pyrazine is added (1.4:1.0 for M:Pyz) and the resonance at 8.63 ppm increases. Within the time required to prepare the solutions and carry out the NMR experiment, it is clear that the monomer has partially aquated to form dimer and free pyrazine. In an aqueous solution dissolved monomer is about 75% and the dimer formed is 25% of the total iron speciation at the same concentration the experiments were done in RMs after about one to two hours as determined from the ratios of the integrations in the $^1\text{H-NMR}$ spectra.

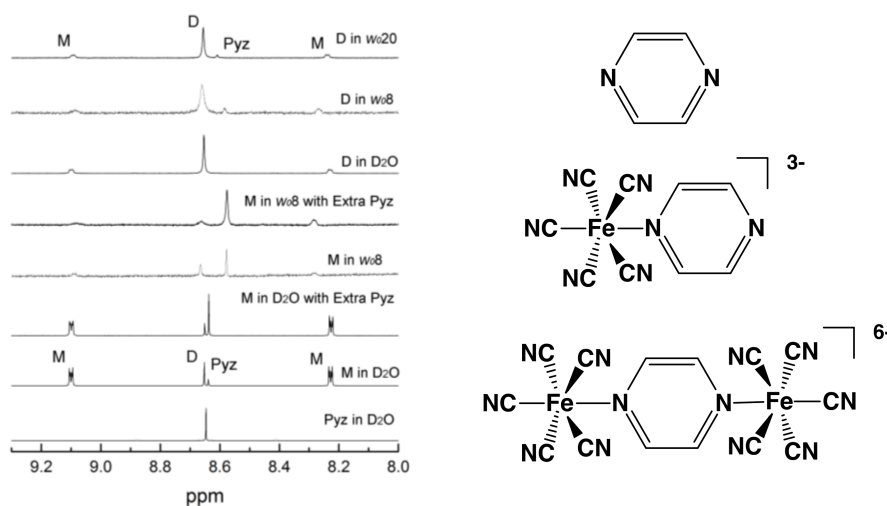


Figure 5. $^1\text{H-NMR}$ spectra recorded at 300 MHz of 20 mM M (or D) in aqueous solution, or in 0.75 M AOT /isooctane RMs. Starting from the bottom: Pyz in D_2O , M in D_2O , M in D_2O spiked with Pyz; RM size w_0 8 and RM spiked with Pyz; D in D_2O ; D in RM w_0 8 and w_0 20. The structures of pyrazine (abbreviated Pyr), the monomeric pentacyano(pyrazine)ferrate(II) $[\text{Fe}(\text{CN})_5(\text{pyrazine})]^{3-}$ (abbreviated M) and the dimeric $[\text{Fe}(\text{CN})_5(\text{pyrazine})\text{Fe}(\text{CN})_5]^{6-}$ (abbreviated D) are shown.

We found that placing the monomer into an AOT/isooctane RMs rapidly decreases the monomer signal in the spectra with a concomitant increase in the dimer and free pyrazine signals. Because the peak positions shifted from those found in D_2O , spiking experiments with pyrazine were again carried out to identify the free pyrazine peak. In a w_0 8 RM the resonances of the monomer and dimer were shifted only slightly. The monomer is now at 9.02 and 8.27 ppm and the dimer is at 8.66 ppm. These small changes (~ 0.06 ppm) support that there is little direct interaction with the AOT interface, as suggested by the lack of change of the MLCT band in the visible spectrum. Likewise, the free pyrazine shifts from 8.63 to 8.58 ppm, which also indicates it remains in the water pool of the RM. In experiments with aniline in RMs, the resonances shift as much as 0.3 ppm between bulk water and in w_0 10 RMs [29]. Similar shifts would be expected for the free and the monomer pyrazine resonances between D_2O and RM w_0 8 if the Pyz was associated with the interface. Similar observations would be made if smaller ionic shells encapsulate ionic pools which provide smaller organized water pools that rigidly stabilized the iron complexes.

Similarly, the top three spectra in Figure 5 show the dimer in D_2O , the dimer in an AOT/isooctane RM, and the dimer in an AOT/isooctane RM with extra Pyz added. These spectra demonstrate the chemical shifts for the dimer in D_2O and a w_0 8 RM are essentially identical. This suggests that the dimer is in the water pool with little interaction between the interface and the pyrazine bridge. In both w_0 8 and 20 RMs, a distribution of monomer and dimer occurred and were similar to those when monomer undergoes hydrolysis to form the dimer. This supports the possibility that the dimer is stabilized with respect to the monomer in RMs.

Experiments were carried out to ascertain the effect of RM size variation on the distribution of the monomer and dimer in the water pool. Figure 6 shows $^1\text{H-NMR}$ spectra recorded for the monomer and dimer in the water pool. Figure 6 shows $^1\text{H-NMR}$ spectra recorded for the monomer in varying w_0 s (8, 10, and 20) with the position of the chemical shifts in D_2O for comparison. In the RMs of w_0 8 and 10, the doublet signals for the monomer shift from those in D_2O but not for w_0 20. Similarly, the dimer shifts at w_0 8 and 10 but not at w_0 20. This shows that the probes reside in the water pool and that the “aqueous” environment, e.g., the solvation, at w_0 20 is similar to that in bulk aqueous media. The shifts of ~ 0.06 ppm observed in the smaller w_0 s can be rationalized by a change in the nature of water in aqueous core as the size is decreasing as well as the ion pairing due to the increased concentration of the sodium ions from the AOT surfactant. This ion pairing may result in more “rigidity” of the dimer structure via charge neutralization.

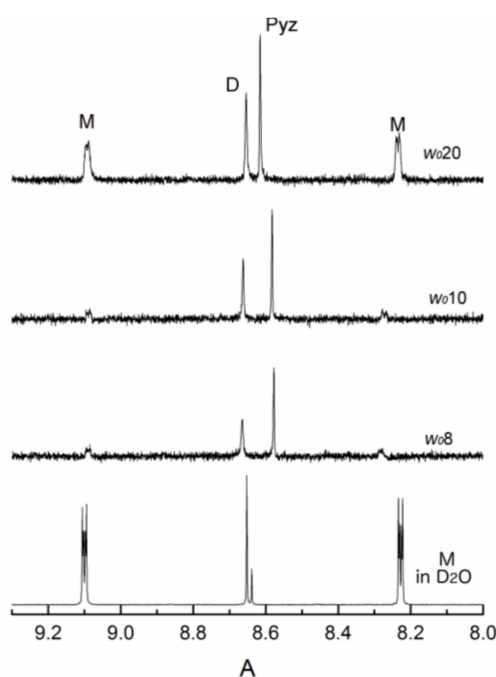


Figure 6. $^1\text{H-NMR}$ spectra recorded at 300 MHz of 0.020 M and in 0.75 M AOT/isooctane at pH 8.82. Starting from the bottom: M in D_2O , M in RM sizes w_0 8, 10, and 20. Spectra were taken approximately 30 min after preparation of the mixture.

Our data are consistent with the monomer and the dimer residing in the water pool, although the possibility of interface proximity and some interaction at the interface cannot be completely discounted. Penetration of the complex or its pyrazine ligand into the negatively charged interfacial region however, seems unlikely, particularly for the high negatively charged dimer. Similar conclusions about changes in the core water, hence solvation, have been suggested for other AOT-iso-octane RM studies [26,46–49]. In contrast, the free pyrazine is shifted at all values measured as compared to bulk D_2O . While not definitive, this suggests that pyrazine may reside closer to the interfacial regions between bulk water and the AOT head groups compared to the complexes. This difference between free and coordinated pyrazine is not unexpected since the metal complexes possess negative charges that will be electrostatically repelled by the negatively charged AOT head groups whereas the neutral pyrazine can move freely and associate favorably in the less polar interfacial region of the interface.

The ratio of monomer and dimer signals are dramatically altered upon confinement within the RM. The line broadening of the monomer and the dimer signals in the RMs suggest that the mobility of the complexes is significantly changed compared to the aqueous solution. The $^1\text{H-NMR}$ spectra were recorded with different relaxation times (from 0.5 to 2 s) to prevent using inappropriate parameters when comparing the integration of the signals in different RM values to determine the

ratios. Specifically, the integration ratios of the peaks in these spectra give a monomer:dimer ratio of 1.4 for D₂O and 1.1, 0.13, 0.14 for w_0 20, 10, and 8, respectively. At small RM sizes, the monomer is almost completely converted into the dimer resulting in very small ratios so even if there are small change in the T_1 values as the RM size decrease (data not shown), the observed pattern holds.

Figure 7 shows the ¹H-NMR of the dimer in D₂O and in two AOT/isooctane RMs sizes. These spectra compare to a similar series of spectra previously shown in Figure 5. As expected, the aqueous solution shows the prominent signal for the dimer signal and minor signals for the monomer. The ratios of the monomer and dimer integrations equal 0.11 for both w_0 8 and 20. This ratio (0.13) is close to the ratio of the peaks measured when dissolving the monomer into solution. These two results support the UV-Vis studies in concluding that the dimer is stabilized over the monomer in RMs which is opposite that found in bulk water. In contrast to the spectra recorded from samples beginning with the monomer, the ratios of the dimer:monomer remain relatively constant even at w_0 8, where the monomer was unstable (see Figures 5 and 6). However, the increase in linewidth on placement in the RM is consistent with a significant decrease in the relaxation time and a decreased tumbling rate in the RMs. Comparing the spectra of w_0 8 and 20 show the increased linewidth at the smaller RM and decreased tumbling in these smaller RMs. The appearance of a peak at 8.63 ppm corresponds to the formation of some free pyrazine that formed from the dissociation of the dimer. This supports our previous observations that the dimer is stabilized within a RM and only a little dimer is hydrolyzed when placed in the RM.

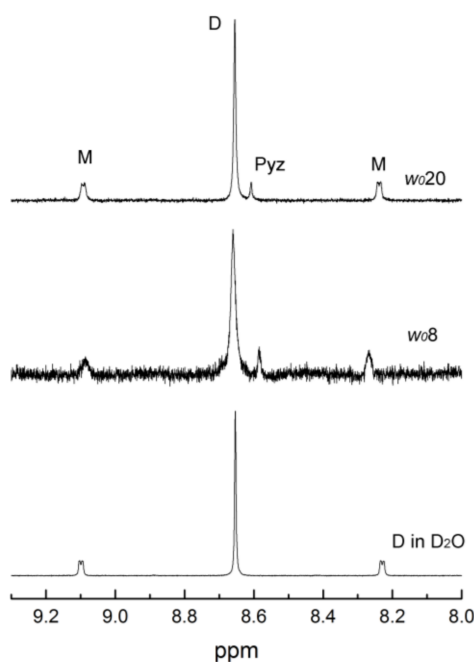


Figure 7. ¹H-NMR spectra were recorded at 300 MHz of a pH 9.0 solution D (0.020 mM) in aqueous solution and in 0.75 M AOT/isooctane RMs at w_0 sizes 8, 10 and 20. All spectra were taken within 30 min of preparation.

The significantly increased stability of the dimer in RMs, at the expense of the monomer, was not anticipated even though entropically, dimer would be favored over monomer. The decreased stability of the monomer with a 3-charge compared to the dimer with a 6-charge inside a RM with a negatively charged headgroup is however conceptually unexpected, and the observation could not be explained based on changes in concentration as the size of the RM changed. Using standard bond lengths, the diameters of the complexes range from 5–6 Å for the monomer to 13–15 Å for the dimer. The size of the RM waterpool have previously been reported [32] to have a diameter of 32 Å for the w_0 8 and 70 Å

for the w_0 20. The size of the RM can be measured using Dynamic Light Scattering (DLS), and thus include both the waterpool and the interfacial layer of the surfactant. However, as the size approaches w_0 8, the dimer fills the entire RM with a shell of water molecules between the compound and the interface of the RM.

We have previously shown that V_{10} with a 6-charge is stable inside RMs and forms even when initially protonated [50]. We found that RMs could not be formed below w_0 5 or 6 in that system. This size allowed for a V_{10} molecule and a layer of 2–3 water molecules inside the water droplet. We also showed that a V_{10} with a Mo [51] replacing one of the V-atoms, $V_9\text{Mo}$, with similar shape but at a different charge behave similarly to V_{10} [50,51]. These compounds are placed in the center of the water pool, however, we found that cations could change the system significantly [52]. Similarly, it was demonstrated that the interacting of water in NaAOT is compromised and that by comparison to the ionic liquid-like surfactant 1-butyl-3-methylimidazolium 1,4-bis-2-ethylhexylsulfosuccinate RMs in benzene that H-bonding has been disrupted in the NaAOT nanostructures [53]. Compounds such as aniline [29], phenol [50] or 1-phenylbiguanide [54] are found to associate closely with the interface, and thus it is possible that Pyr would similarly associate with the interface. Indeed, a recent molecular dynamic study has shown that there is strong interaction between solvent molecules at the interface region [55].

In conclusion, these types of studies are important for investigation of reactions in RMs. Specifically, protonation reactions [56–59], nucleophilic substitution reactions [60–64], electron transfer reactions [26–29], and enzymatic reactions [65–67] have been investigated and are known to be affected by the inhomogeneous environment such as those found in microemulsions.

3. Materials and Methods

3.1. General Materials and Methods

Chemicals were used as obtained or as in the case of sodium bis(ethylhexyl)succinate (also named dioctylsulfosuccinate sodium salt abbreviated NaAOT) purified according to previous methods [68]. All of the following chemicals were obtained from: NaAOT (Sigma-Aldrich (98% purity St. Louis, MO, USA), deuterium oxide (Cambridge Isotope Laboratories Inc., 99.9%, Tewksbury, MA, USA), 3-(trimethylsilyl)-1-propanesulfonic acid sodium salt (DSS) (Willard 99.9%, Frederick, MD, USA), 2,2,4-trimethylpentane (or isooctane) (Sigma-Aldrich ACS Reagent grade + 99.0%), methanol (EMD HPLC Grade 99.9%), pyrazine (Aldrich 99+% abbreviated pyz), d^6 -dimethylsulfoxide (Cambridge Isotope Laboratories Inc., 99.9% + 0.05% *v/v* TMS). The dimer, $\text{Na}_6[\text{Fe}_2(\text{CN})_{10}\text{pyz}]$ and the monomer, $\text{Na}_3[\text{Fe}(\text{CN})_5\text{pyz}]$ were synthesized and characterized as reported in the literature [44,45].

3.2. Preparation of Solutions

3.2.1. Metal Complex Solutions

Aqueous solutions were prepared by dissolving the monomer or dimer into either 100% D_2O or 10% D_2O , unless otherwise indicated. The pH was adjusted using DCl or NaOD as needed. The pD values were measured with a pH meter and converted to pH by the relationship $\text{pH} = \text{pD} + 0.40$ [29].

3.2.2. Reverse Micelle (RM) Solutions for Spectroscopic Measurements

Microemulsions of RMs were made using purified AOT and were prepared as a 0.75 M AOT/Isooctane solution. Subsequently, the appropriate amount of water (or aqueous probe solution) was added to form the desired RM size (w_0 value = $[\text{H}_2\text{O}]/[\text{AOT}]$) [32,69]. Residual amounts of water in the NaAOT preparation was accounted for in the reported w_0 values and were generally around 0.25–0.30 water molecules for each AOT molecule. UV-Vis measurements were made using similarly prepared RMs, but the total AOT concentration was 0.20 M. The monomer or dimer was added to the RM using a water (or D_2O)/complex solution in place of the pure water (or D_2O). The resulting

mixture was then vortexed until the solution was transparent. These samples were then immediately subjected to investigation by NMR spectroscopic methods.

3.3. Methods

3.3.1. UV-Visible Spectroscopy

Solutions for analysis was prepared as described above. The concentrations of the metal complex ranged between $5\text{--}10 \times 10^{-5}$ M. The UV-Vis spectra were collected using an HP8452A spectrometer (Waltham, MA, USA). Spectra were recorded within 1 min after mixing and at various times thereafter. The spectrometer was referenced using solutions of “empty” RMs at the same w_0 size as those being studied containing the probe. This blank was found to give better baseline readings than recording against air. The use of a “blank” is necessary since there is some light scattering due to the RMs in solution [39].

3.3.2. ^1H -NMR Spectroscopy

^1H -NMR spectra were recorded using a 300 or 400 MHz NMR Varian spectrometer (Palo Alto, CA, USA). Spectra for the monomer and dimer RM solutions were replicated three times. Samples were made fresh each time and immediately shielded from light. Spectra were recorded within 10 min of mixing unless otherwise indicated; significant changes in samples were observed over 30 min to 1 h. The parameters use for recording these spectra in RMs had sweep widths of 5200 Hz, relaxation delays of 1.0 s and a $45\text{--}60^\circ$ pulse angle. The samples were locked on D_2O (100%) and referenced against an AOT/isooctane signal which had previously been referenced against a solution of DSS as described previously [27].

3.3.3. Dynamic Light Scattering (DLS)

DLS measurements were done to confirm that RMs formed and that they were of the sizes reported previously [32].

4. Conclusions

In this study, we have demonstrated that a confined environment affects the stability of simple coordination complexes, i.e., their ligand exchange equilibria, along with their speciation. We observed that the complexation rates are increased as the size of the RM decreases and that the dimeric form of the complex is the preferred species in the reverse micellar environment in contrast to bulk water where the monomer is the dominant species.

The changes observed in the NMR spectra, and differences in equilibria, for the different complex forms added to a variety of RM sizes could be due to environmental factors within the RMs. Specifically, the solvation of the metal complexes may control their hydrolysis rates and speciation as the size of the RM changes. At low w_0 values, there are fewer water molecules and these are used primarily to solvate the sodium ions and AOT headgroups [32], thus forming the RM. Introduction of a metal complex will compete for these waters and change its dynamics. The shifting NMR peaks observed between water and in different RMs is consistent with this conclusion, although the observed changes may also be in part due, in part, to increased ion pairing with the sodium ions or interactions with the RM headgroups. Nevertheless, it is clear that the environment in which the metal complex is confined differs significantly from bulk water.

This study imparts insight into how metal complexes behave at interfaces and as solvation is altered at the nanoscale. These insights will be important in the understanding of how molecular species are affected and interact at interfaces or membranes within biological, geological, or industrial systems [70–76].

Acknowledgments: The work as funded by New Mexico State University to M.D.J. and by Colorado State University to D.C.C. Partial funding was also provided to M.D.J. from NSF and from the Arthur Cope Foundation to D.C.C. Funds for to publish in open access was obtained by publisher. The authors are grateful to the helpful suggestions of the reviewers of this manuscript.

Author Contributions: M.D.J. and D.C.C. conceived, designed and supervised the experiments; T.B. and A.J.M. performed the UV-Vis and kinetic experiments; M.J.F. performed the NMR spectroscopic experiments; M.D.J. and D.C.C. analyzed the data; M.D.J. and D.C.C. wrote the paper.

Conflicts of Interest: The authors declare no conflict of interest.

References

1. Ferreira, P.; Xue, W.-M.; Bencze, E.; Herdtweck, E.; Kuehn, F.E. Bidentate Lewis Base Adducts of Methyltrioxorhenium(VII) and Their Application in Catalytic Epoxidation. *Inorg. Chem.* **2001**, *40*, 5834–5841. [[CrossRef](#)] [[PubMed](#)]
2. Hratchian, H.P.; Sonnenberg, J.L.; Hay, P.J.; Martin, R.L.; Bursten, B.E.; Schlegel, H.B. Theoretical Investigation of Uranyl Dihydroxide: Oxo Ligand Exchange, Water Catalysis, and Vibrational Spectra. *J. Phys. Chem. A* **2005**, *109*, 8579–8586. [[CrossRef](#)] [[PubMed](#)]
3. Moloney, M.G.; Paul, D.R.; Thompson, R.M.; Wright, E. Ligand exchange and catalysis in phenylation reactions mediated by lead tetracarboxylates. *J. Organomet. Chem.* **1998**, *560*, 77–88. [[CrossRef](#)]
4. Ortiz-Maldonado, M.; Ballou, D.P.; Massey, V. A Rate-Limiting Conformational Change of the Flavin in *p*-Hydroxybenzoate Hydroxylase Is Necessary for Ligand Exchange and Catalysis: Studies with 8-Mercapto- and 8-Hydroxy-Flavins. *Biochemistry* **2001**, *40*, 1091–1101. [[CrossRef](#)] [[PubMed](#)]
5. Basolo, F. Base hydrolysis of cobalt (III) ammines. *Bull. Hist. Chem.* **1996**, *19*, 66–71.
6. Wilkins, R.G. Factors influencing the rates of dissociation of metal complexes. IV. A comparison of nickel(II)- and copper(II)diamine complexes. *J. Chem. Soc.* **1962**, 4475–4478. [[CrossRef](#)]
7. Hubbard, C.D.; Van Eldik, R. Mechanistic studies of reactions of coordination compounds. Some recent highlights. *J. Coord. Chem.* **2007**, *60*, 1–51. [[CrossRef](#)]
8. Swaddle, T.W. *Ligand Substitution Dynamics in Metal Complexes*; John Wiley & Sons, Inc.: Hoboken, NJ, USA, 2010; pp. 339–393. [[CrossRef](#)]
9. Lincoln, S.E. Mechanistic studies of metal aqua ions: A semi-historical perspective. *Helv. Chim. Acta* **2005**, *88*, 523–545. [[CrossRef](#)]
10. Richens, D.T. Ligand substitution reactions at inorganic centers. *Chem. Rev.* **2005**, *105*, 1961–2002. [[CrossRef](#)] [[PubMed](#)]
11. Macartney, D.H. Properties and reactions of substituted pentacyanoferrate(II) complexes. *Rev. Inorg. Chem.* **1988**, *9*, 101–151. [[CrossRef](#)]
12. Wilkins, R.G. *The Study of Kinetics and Mechanism of Reactions of Transition Metal Complexes*; Allyn and Bacon: Boston, MA, USA, 1974; p. 403.
13. Bachmann, P.A.; Walde, P.; Luisi, P.L.; Lang, J. Self-replicating micelles: Aqueous micelles and enzymatically driven reactions in reverse micelles. *J. Am. Chem. Soc.* **1991**, *113*, 8204–8209. [[CrossRef](#)]
14. Gupte, A.; Nagarajan, R.; Kilara, A. Enzyme reactions in reverse micelles. *Dev. Food Sci.* **1995**, *37A*, 1–74. [[CrossRef](#)]
15. Li, Y.; Li, G.; Ma, C. Enzymology in surfactant association systems. *J. Dispers. Sci. Technol.* **2000**, *21*, 409–432. [[CrossRef](#)]
16. Wang, Y.; Wu, J.; Ru, X.; Jiang, Y.; Hu, M.; Li, S.; Zhai, Q. Catalytic performance and thermostability of chloroperoxidase in reverse micelle: Achievement of a catalytically favorable enzyme conformation. *J. Ind. Microbiol. Biotechnol.* **2011**, *38*, 717–724. [[CrossRef](#)] [[PubMed](#)]
17. Crans, D.C.; Trujillo, A.M.; Pharazyn, P.S.; Cohen, M.D. How environment affects drug activity: Localization, compartmentalization and reactions of a vanadium insulin-enhancing compound, dipicolinatooxovanadium(V). *Coord. Chem. Rev.* **2011**, *255*, 2178–2192. [[CrossRef](#)]
18. O'Connor, C.J.; Fendler, E.J.; Fendler, J.H. Catalysis by reversed micelles in nonplanar solvents. Aquation and electron-transfer reactions of chromium(III) and cobalt(III) complexes in benzene. *J. Chem. Soc. Dalton Trans.* **1974**, 625–631. [[CrossRef](#)]
19. O'Connor, C.J.; Fendler, E.J.; Fendler, J.H. Catalysis by reversed micelles in nonpolar solvents. Trans-cis isomerization of bis(oxalato)diaquochromate(III). *J. Am. Chem. Soc.* **1974**, *96*, 370–375. [[CrossRef](#)]

20. Burgess, J.; Patel, M.S. Pentacyanoferrates(II): Solvatochromism and reactivity in micelles and in reversed micelles. *J. Chem. Soc. Faraday Trans.* **1993**, *89*, 783–787. [[CrossRef](#)]
21. Yamagishi, A.; Masui, T.; Watanabe, F. Temperature-jump studies of the ligand substitution reactions of tetrahedral cobalt(II) complexes solubilized in reversed micelles. *Inorg. Chem.* **1981**, *20*, 513–518. [[CrossRef](#)]
22. Venkateswarlu, G.; Syamala, P.; Rao, P.V.S.; Ramakrishna, K. Kinetics of dissociation of tris(1,10-phenanthroline)iron(II) in aqueous and reverse micellar media—Catalysis of CuII, NiII and CoII ions. *J. Indian Chem. Soc.* **2003**, *80*, 86–90.
23. Baruah, B.; Roden, J.M.; Sedgwick, M.; Correa, N.M.; Crans, D.C.; Levinger, N.E. When is water not water? Exploring water confined in large reverse micelles using a highly charged inorganic molecular probe. *J. Am. Chem. Soc.* **2006**, *128*, 12758–12765. [[CrossRef](#)] [[PubMed](#)]
24. Stover, J.; Rithner, C.D.; Inafuku, R.A.; Crans, D.C.; Levinger, N.E. Interaction of dipicolinatodioxovanadium(V) with polyatomic cations and surfaces in reverse micelles. *Langmuir* **2005**, *21*, 6250–6258. [[CrossRef](#)] [[PubMed](#)]
25. Chatkon, A.; Barres, A.; Samart, N.; Boyle, S.; Haller, K.J.; Crans, D.C. Guanylurea metformium double salt of decavanadate, (HGU⁺)₄(HMet⁺)₂(V₁₀O₂₈⁶⁻)·2H₂O. *Inorg. Chem. Acta* **2014**, *420*, 85–91. [[CrossRef](#)]
26. Crans, D.C.; Baruah, B.; Gaidamauskas, E.; Lemons, B.G.; Lorenz, B.B.; Johnson, M.D. Impairment of ascorbic acid's anti-oxidant properties in confined media: Inter and intramolecular reactions with air and vanadate at acidic pH. *J. Inorg. Biochem.* **2008**, *102*, 1334–1347. [[CrossRef](#)] [[PubMed](#)]
27. Johnson, M.D.; Lorenz, B.B.; Wilkins, P.C.; Lemons, B.G.; Baruah, B.; Lamborn, N.; Stahla, M.; Chatterjee, P.B.; Richens, D.T.; Crans, D.C. Switching off Electron Transfer Reactions in Confined Media: Reduction of [Co.(dipic)2]- and [Co.(edta)]- by Hexacyanoferrate(II). *Inorg. Chem.* **2012**, *51*, 2757–2765. [[CrossRef](#)] [[PubMed](#)]
28. Lemons, B.G.; Richens, D.T.; Anderson, A.; Sedgwick, M.; Crans, D.C.; Johnson, M.D. Stabilization of a vanadium(V)-catechol complex by compartmentalization and reduced solvation inside reverse micelles. *New J. Chem.* **2013**, *37*, 75–81. [[CrossRef](#)]
29. Lemons, B.G.; Crans, D.C.; Johnson, M.D. Electron transfer rate enhancements in nanosized waterpools. *Eur. J. Inorg. Chem.* **2014**, *27*, 4537–4540. [[CrossRef](#)]
30. Molina, P.G.; Silber, J.J.; Correa, N.M.; Sereno, L. Electrochemistry in AOT Reverse Micelles. A Powerful Technique to Characterize Organized Media. *J. Phys. Chem. C* **2007**, *111*, 4269–4276. [[CrossRef](#)]
31. De, T.; Maitra, A. Solution behavior of Aerosol OT in non-polar solvents. *Adv. Colloid Interface Sci.* **1995**, *59*, 95–193. [[CrossRef](#)]
32. Maitra, A. Determination of size parameters of water aerosol OT oil reverse micelles from their nuclear magnetic resonance data. *J. Phys. Chem.* **1984**, *88*, 5122–5125. [[CrossRef](#)]
33. Gaidamauskas, E.; Cleaver, D.P.; Chatterjee, P.B.; Crans, D.C. Effect of Micellar and Reverse Micellar Interface on Solute Location: 2,6-Pyridinedicarboxylate in CTAB Micelles and CTAB and AOT Reverse Micelles. *Langmuir* **2010**, *26*, 13153–13161. [[CrossRef](#)] [[PubMed](#)]
34. Park, S.; Moilanen, D.E.; Fayer, M.D. Water dynamics—The effects of ions and nanoconfinement. *J. Phys. Chem. B* **2008**, *112*, 5279–5290. [[CrossRef](#)] [[PubMed](#)]
35. Belafi-Bako, K.; Nagy, E. Characteristics of AOT/isooctane/water system. *Hung. J. Ind. Chem.* **1994**, *22*, 51–56.
36. Boyer, B.; Lamaty, G.; Mary, F.; Mouanga, J.; Roque, J.P. Reactivity in reverse micelles. Effects of micelle size and the role of the cosurfactant. *New J. Chem.* **1992**, *16*, 375–379.
37. Fayer, M.D.; Levinger, N.E. Analysis of Water in Confined Geometries and at Interfaces. *Ann. Rev. Anal. Chem.* **2010**, *3*, 89–107. [[CrossRef](#)] [[PubMed](#)]
38. Piletic, I.R.; Moilanen, D.E.; Spry, D.B.; Levinger, N.E.; Fayer, M.D. Testing the core/shell model of nanoconfined water in reverse micelles using linear and nonlinear IR spectroscopy. *J. Phys. Chem. A* **2006**, *110*, 4985–4999. [[CrossRef](#)] [[PubMed](#)]
39. Day, R.A.; Robinson, B.H.; Julian, H.R.; Clarke, J.H.R.; Doherty, J.V. Characterisation of water-containing reversed micelles by viscosity and dynamic light scattering methods. *J. Chem. Soc. Faraday Trans. 1* **1979**, *75*, 132–139. [[CrossRef](#)]
40. Crans, D.C.; Baruah, B.; Ross, A.; Levinger, N.E. Impact of confinement and interfaces on coordination chemistry: Using oxovanadate reactions and proton transfer reactions as probes in reverse micelles. *Coord. Chem. Rev.* **2009**, *253*, 2178–2185. [[CrossRef](#)]

41. Ooms, K.J.; Bolte, S.E.; Baruah, B.; Choudhary, M.A.; Crans, D.C.; Polenova, T. V-51 solid-state NMR and density functional theory studies of eight-coordinate non-oxo vanadium complexes: Oxidized amavadin. *Dalton Trans.* **2009**, 3262–3269. [[CrossRef](#)]
42. Durantini, A.M.; Falcone, R.D.; Silber, J.J.; Correa, N.M. A New Organized Media: Glycerol:*N,N*-Dimethylformamide Mixtures/*AOT/n*-Heptane Reversed Micelles. The Effect of Confinement on Preferential Solvation. *J. Phys. Chem. B* **2011**, *115*, 5894–5902. [[CrossRef](#)] [[PubMed](#)]
43. Malin, J.M.; Schmidt, C.F.; Toma, H.E. Carbon-13 and proton nuclear magnetic resonance spectra of some pentacyanoferrate(II) complexes. *Inorg. Chem.* **1975**, *14*, 2924–2928. [[CrossRef](#)]
44. Felix, F.; Hauser, U.; Siegenthaler, H.; Wenk, F.; Ludi, A. Mixed valence properties of μ -pyrazine-decacyanodiiron(II, III). *Inorg. Chim. Acta* **1975**, *15*, L7–L8. [[CrossRef](#)]
45. Toma, H.E.; Malin, J.M. Kinetics of formation and stability constants of some pentacyanoferrate(II) complexes of aromatic nitrogen heterocycles. *Inorg. Chem.* **1973**, *12*, 2080–2083. [[CrossRef](#)]
46. Willard, D.M.; Riter, R.E.; Levinger, N.E. Dynamics of polar solvation in lecithin/water/cyclohexane reverse micelles. *J. Am. Chem. Soc.* **1998**, *120*, 4151–4160. [[CrossRef](#)]
47. Raju, B.B.; Costa, S.M.B. Excited-state behavior of 7-diethylaminocoumarin dyes in *AOT* reversed micelles: Size effects. *J. Phys. Chem B* **1999**, *103*, 4309–4317. [[CrossRef](#)]
48. Crans, D.C.; Trujillo, A.M.; Bonetti, S.; Rithner, C.D.; Baruah, B.; Levinger, N.E. Penetration of Negatively Charged Lipid Interfaces by the Doubly Deprotonated Dipicolinate. *J. Org. Chem.* **2008**, *73*, 9633–9640. [[CrossRef](#)] [[PubMed](#)]
49. Zingaretti, L.; Correa, N.M.; Boscatto, L.; Chiacchiera, S.M.; Durantini, E.N.; Bertolotti, S.G.; Rivarola, C.R.; Silber, J.J. Distribution of amines in water/*AOT/n*-hexane reverse micelles: Influence of the amine chemical structure. *J. Colloid Interface Sci.* **2005**, *286*, 245–252. [[CrossRef](#)] [[PubMed](#)]
50. Crans, D.C.; Rithner, C.D.; Baruah, B.; Gourley, B.L.; Levinger, N.E. Molecule probe location in reverse micelles determined by NMR dipolar interactions. *J. Am. Chem. Soc.* **2006**, *128*, 4437–4445. [[CrossRef](#)] [[PubMed](#)]
51. Sánchez-Lombardo, I.; Baruah, B.; Alvarez, S.; Werst, K.R.; Segaline, N.A.; Levinger, N.E.; Crans, D.C. Size and shape trump charge in interactions of oxovanadates with self-assembled interfaces: Application of Continuous Shape Measure analysis to the decavanadate anion. *New J. Chem.* **2016**, *40*, 962–975. [[CrossRef](#)]
52. Samart, N.; Beuning, C.; Haller, K.; Rithner, C.D.; Crans, D.C. Interaction of a biguanide compound with membrane model interface systems: Probing properties of antimalaria and antidiabetic compounds. *Langmuir* **2014**, *30*, 8697–8706. [[CrossRef](#)] [[PubMed](#)]
53. Lepori, C.M.O.; Correa, N.M.; Silber, J.J.; Falcone, R.D. How the cation 1-butyl-3-methylimidazolium impacts the interaction between the entrapped water and the reverse micelles interface created with an ionic liquid-like surfactant. *Soft Matter* **2016**, *12*, 830–844. [[CrossRef](#)] [[PubMed](#)]
54. Silva, F.O.; Fernandez, M.A.; Silber, J.J.; de Rossi, R.H.; Correa, N.M. Inhibited phenol ionization in reverse micelles: Confinement effect at the nanometer scale. *Chemphyschem* **2012**, *13*, 124–130. [[CrossRef](#)] [[PubMed](#)]
55. Agazzi, F.; Correa, N.M.; Rodriguez, J. Molecular dynamic simulation of water/BHDC cationic reverse micelles. Structural characterization, dynamical properties, and influence of solvent on intermicellar interactions. *Langmuir* **2014**, *30*, 9643–9653. [[CrossRef](#)] [[PubMed](#)]
56. Crans, D.C.; Levinger, N.E. The conundrum of pH in water nanodroplets: Sensing pH in reverse micelle water pools. *Acc. Chem. Res.* **2012**, *45*, 1637–1645. [[CrossRef](#)] [[PubMed](#)]
57. Sedgwick, M.; Cole, R.L.; Rithner, C.D.; Crans, D.C.; Levinger, N.E. Correlating Proton Transfer Dynamics to Probe Location in Confined Environments. *J. Am. Chem. Soc.* **2012**, *134*, 11904–11907. [[CrossRef](#)] [[PubMed](#)]
58. Sripradite, J.; Miller, S.A.; Johnson, M.D.; Tongraar, A.; Crans, D.C. How Interfaces Affect the Acidity of the Anilinium Ion. *Chem. Eur. J.* **2016**, *22*, 3873–3880. [[CrossRef](#)] [[PubMed](#)]
59. Levinger, N.E.; Rubenstrunk, L.C.; Baruah, B.; Crans, D.C. Acidification of reverse micellar nanodroplets by CO₂. *J. Am. Chem. Soc.* **2011**, *133*, 7205–7213. [[CrossRef](#)] [[PubMed](#)]
60. Blach, D.; Pessego, M.; Silber, J.J.; Correa, N.M.; Garcia-Río, L.; Falcone, R.D. Ionic liquids entrapped in reverse micelles as nanoreactors for bimolecular nucleophilic substitution reaction. Effect of the confinement on the chloride ion availability. *Langmuir* **2014**, *30*, 12130–12137. [[CrossRef](#)] [[PubMed](#)]
61. Crosio, M.A.; Correa, N.M.; Silber, J.J.; Falcone, R.D. Aprotic ionic liquid, when entrapped in cationic reverse micelles, can be used as a suitable solvent for a bimolecular nucleophilic substitution reaction. *Org. Biomol. Chem.* **2016**, *14*, 3170–3177. [[CrossRef](#)] [[PubMed](#)]

62. Correa, N.M.; Durantini, E.N.; Silber, J.J. Influence of anionic and cationic reverse micelles on nucleophilic aromatic substitution reactions between 1-fluoro-2,4-dinitrobenzene and piperidine. *J. Org. Chem.* **2000**, *65*, 6427–6433. [[CrossRef](#)] [[PubMed](#)]
63. Crans, D.C.; Schoeberl, S.; Gaidamauskas, E.; Baruah, B.; Roess, D.A. Antidiabetic vanadium compound and membrane interfaces: Interface facilitated metal complex hydrolysis. *J. Biol. Inorg. Chem.* **2011**, *16*, 961–972. [[CrossRef](#)] [[PubMed](#)]
64. Chatkon, A.; Chatterjee, P.B.; Sedgwick, M.A.; Haller, K.J.; Crans, D.C. Counterion affects interaction with interfaces: The antidiabetic drugs metformin and decavanadate. *Eur. J. Inorg. Chem.* **2013**, *2013*, 1859–1868. [[CrossRef](#)]
65. Moyano, F.; Setjen, E.; Silber, J.J.; Correa, N.M. Enzymatic hydrolysis of *N*-benzoyl-L-tyrosine *p*-nitroanilide by α -chymotrypsin in DMSO-water/AOT/*n*-heptane reverse micelles. A unique interfacial effect on the enzymatic activity. *Langmuir* **2013**, *29*, 8245–8254. [[CrossRef](#)] [[PubMed](#)]
66. Biasutti, M.A.; Abuin, E.B.; Silber, J.J.; Correa, N.M.; Lissi, E.A. Kinetics of reactions catalyzed by enzymes in solutions of surfactant. *Adv. Colloid Interface Sci.* **2008**, *136*, 1–24. [[CrossRef](#)] [[PubMed](#)]
67. Solis, A.K.C.; Correa, N.M.; Molina, P.G. Determination of benzyl-hexadecyldimethylammonium 1,4-bis(2-ethylhexyl)sulfosuccinate vesicle permeability by using square wave voltammetry and an enzymatic reaction. *Langmuir* **2017**, *33*, 12080–12086. [[CrossRef](#)] [[PubMed](#)]
68. Stahla, M.L.; Baruah, B.; James, D.M.; Johnson, M.D.; Levinger, N.E.; Crans, D.C. ¹H NMR studies of aerosol-OT reverse micelles with alkali and magnesium counterions: Preparation and analysis of MAOTs. *Langmuir* **2008**, *24*, 6027–6035. [[CrossRef](#)] [[PubMed](#)]
69. Zulauf, M.; Eicke, H.-F. Inverted Micelles and Microemulsions in the Ternary-System H₂O-Aerosol-OT-Isooctane as Studied by Photon Correlation Spectroscopy. *J. Phys. Chem.* **1979**, *83*, 480–486. [[CrossRef](#)]
70. Winter, P.W.; Al-Qatati, A.; Wolf-Ringwall, A.; Schoeberl, S.; Van Orden, A.K.; Barisas, B.G.; Roess, D.A.; Crans, D.C. The anti-diabetic bis(maltolato)oxovanadium(IV) (BMOV) reduce insulin receptor lateral diffusion and increase receptor confinement in membrane microdomains. *Dalton Trans.* **2012**, *41*, 6419–6430. [[CrossRef](#)] [[PubMed](#)]
71. Bakas, L.; Verza, G.; Cortizo, A. Effect of vanadium compounds on the lipid organization of liposomes and cell membranes. *Biol. Trace Elem. Res.* **2001**, *80*, 269–279. [[CrossRef](#)]
72. Sarkar, Y.; Majumder, R.; Das, S.; Ray, A.; Parui, P.P. Detection of curvature-radius-dependent interfacial pH/polarity for amphiphilic self-assemblies: positive versus negative curvature. *Langmuir* **2018**. [[CrossRef](#)] [[PubMed](#)]
73. Ishikawa, A.A.; Salazar, J.V.; Salinas, M.; Gaitani, C.M.; Nurkiewicz, T.; Negrete, G.R.; Garcia, C.D. Self-assembled nanospheres for encapsulation and aerosolization of rifampicin. *RSC Adv.* **2016**, *6*, 12959–12963. [[CrossRef](#)] [[PubMed](#)]
74. Pauletti, G.M.; Wunderliallenspach, H. Partition-Coefficients in-Vitro—Artificial Membranes as a Standardized Distribution Model. *Eur. J. Pharm. Sci.* **1994**, *1*, 273–282. [[CrossRef](#)]
75. Ataf, A.A.; Lal, B.; Badshah, A.; Usman, M.; Chatterjee, P.B.; Huq, F.; Ullah, S.; Crans, D.C. Synthesis, structural characterization, modal membrane interaction and anti-tumor cell line studies of nitrophenyl ferrocenes. *J. Mol. Structure.* **2016**, *1113*, 162–170. [[CrossRef](#)]
76. Jain, M.K. *Introduction to Biological Membranes*, 2nd ed.; John Wiley and Sons: New York, NY, USA, 1988.

Sample Availability: Compounds are readily available by synthesis from commercially available material according to literature procedures.



© 2018 by the authors. Licensee MDPI, Basel, Switzerland. This article is an open access article distributed under the terms and conditions of the Creative Commons Attribution (CC BY) license (<http://creativecommons.org/licenses/by/4.0/>).